

Sign and Relevance learning

Sama Daryanavard¹, Bernd Porr¹

¹Biomedical Engineering Division, School of Engineering, University of Glasgow, Glasgow G12 8QQ, UK.

Keywords: neuromodulation, reinforcement learning, deep learning, synaptic plasticity, dopamine, serotonin.

Abstract

Standard models of biologically realistic, or inspired, reinforcement learning employ a global error signal which implies shallow networks. However, deep networks could offer a drastically superior performance by feeding the error signal backwards through such a network which in turn is not biologically realistic as it requires symmetric weights between top-down and bottom-up pathways. Instead, we present a network combining local learning with global modulation where neuromodulation controls the amount of plasticity change in the whole network, while only the sign of the error is backpropagated through the network. The neuromodulation can be understood as a rectified error, or relevance, signal while the bottom-up sign of the error signal decides between long-term potentiation and long-term depression. We demonstrate the performance of this paradigm with a real robotic task.

1 Introduction

The learning of an organism is understood in the context of interactions with its environment facilitated through sensory inputs and motor outputs which, in turn, cause new sensory inputs. The framework for such learning is closed-loop learning ([von Uexküll, 1926](#)) where actions lead to either negative or positive consequences; this is the realm of reinforcement learning ([Dayan and Balleine, 2002](#)). Central to reinforcement learning in a biologically realistic or inspired framework is the reward prediction error. [Schultz et al \(1997\)](#) suggested, in the 90s, that dopamine codes this error ([Bromberg-Martin et al, 2010](#); [Wood et al, 2017](#); [Takahashi et al, 2017](#)) which is reminiscent of the so called temporal difference error in machine learning ([Sutton, 1988](#)). This led to the assumption that the brain resembles an actor / critic architecture where dopamine, as the reward prediction error, drives synaptic changes in the striatum ([Humphries et al, 2006](#)). An-

other interpretation of the actor / critic architecture is a nested closed-loop platform where an inner reflex loop generates an error signal which tunes an actor in an outer loop to create anticipatory actions, in other words, the actor generates a forward model of the reflex (Porr and Wörgötter, 2002). Thus the actor / critic architecture can be used for both model and model free learning.

However, using a global error signal such as the reward prediction error is problematic. Firstly, the biologically inspired architectures are shallow (Humphries et al, 2006; O'Reilly and Frank, 2006), as the error signal affects all neurons, for this reason deep layered structures are not useful. Indeed, the standard models of decision making focus on the striatum which is a single layer decision network innervated by dopamine and receives its input from the cortex (Humphries et al, 2006). However, these models do not employ cortical networks for decision making but only for working memory operations or signal conditioning (O'Reilly and Frank, 2006).

Cortical networks are very plastic as well and are certainly the orbitofrontal and medial-prefrontal cortex are heavily involved in reinforcement learning (Haber et al, 1995; Berthoud, 2004; Rolls and Grabenhorst, 2008). These areas are less innervated by dopamine but by serotonin (Roberts, 2011; Linley et al, 2013) which appears to be a rectified reward prediction error or reward anticipation controlling the level of plasticity (Li et al, 2016). Similarly, one could argue that even in the striatum the negative part of the reward prediction error, represented by dopamine in this structure, has little relevance owing to its low baseline firing (Schultz, 2004; Takahashi et al, 2017). Indeed, it has also been championed as a surprise signal (Redgrave et al, 1999; Schultz, 2016) rather than a reward prediction error. Overall, this suggests that a direct mapping of the theoretical temporal difference error onto a neuromodulator is at best a rectified reward prediction error in the case of dopamine but most likely codes rather subjective reward value or utility (Schultz, 2016). In the case of serotonin it codes reward anticipation (Luo et al, 2015; Li et al, 2016).

One should not forget that the main method by which plasticity is induced is via local learning rules such as Hebbian learning (Hebb, 1949; Bliss and Lomo, 1973) or spike timing dependent plasticity (Markram et al, 1997) with its underlying postsynaptic calcium dynamics where a strong concentration of calcium causes long-term potentiation (LTP) and a small concentration causes long-term depression (LTD) (Lu et al, 2001; Castellani et al, 2001). These are local learning rules and they interact with the global neuromodulation (Mattson et al, 2004; Lovinger, 2010).

Recently, in machine learning deep learning has been used for reinforcement learning where an error is propagated back through a network which allows computations in deep network structures (Daryanavard and Porr, 2020). However, deep learning at its core is not biologically realistic, requiring the backpropagation of an error signal which, in turn, demands symmetric weights of the up- and downstream pathways. Several approximations have been attempted to retrofit this property onto biology (Pozzi et al, 2020; Lillicrap et al, 2016a; Stork, 1989).

Another issue is the exploding and vanishing gradient problem (EVGP) (Rehmer and Kroll, 2020; Pascanu et al, 2013; Bengio et al, 1994). While this can be solved elegantly in machine learning with rectifying linear units, real neurons hardly operate as a strict rectifying unit. However, it is clear that biology masters the use of multi-layered networks with ease. It is also clear that they use neuromodulators such as dopamine and sero-

tonin both of which certainly speed up or slow down plasticity. This calls for a network which is still able to propagate errors backwards and in addition uses neuromodulators to control globally plasticity. Whilst a full propagation of the error is very unlikely, simple local LTP or LTD backpropagation is considerably more feasible. We argue here, in line with [Rolls \(2016\)](#), that the upstream error signal can determine the sign of learning (i.e LTP vs LTD) in the downstream network by excitation of their dendrites while the global (rectified) neuromodulator controls the amount of plasticity changes but not its sign.

In this paper, we present a novel network learning mechanism which we believe is closer to biology by combining local and global learning rules. Our network merely performs backpropagation of the *sign* of an error signal, deciding upon LTP or LTD while a global neuromodulation controls the speed of learning. As a proof of concept we employ a simple line following task deployed on a real robot whose deviation generates an error signal used to train the network.

2 The sign and relevance (SaR) learning platform

The sign and relevance (SaR) learning platform is presented in Figure 1. The reflex mechanism, the learner, and the flow of signals are described below.

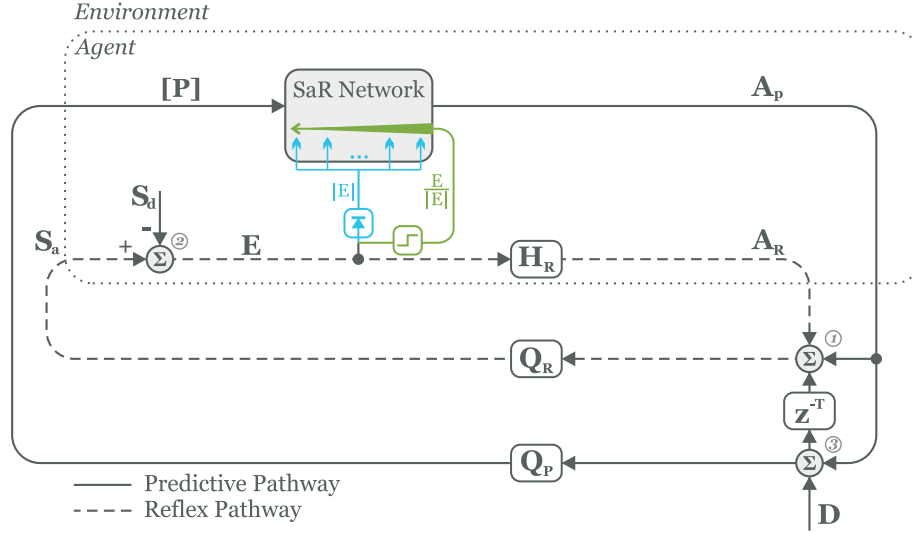


Figure 1: *SaR learning platform. The boundary of the agent and the environment is marked with a dotted rectangle. The platform consists of two loops: the inner reflex loop, shown with dashed lines, and the outer predictive (or learning) loop, shown with solid lines.*

2.1 The reflex loop

As a result of encountering a disturbance, such as a bend in the road when driving, the innate reflex mechanism provides the organism with an immediate reaction so as to correct for the disturbance; this is an involuntary action without prior knowledge. The reflex is a fixed closed-loop controller that opposes disturbance D in order to maintain its desired state S_d . When travelling through the reflex environment Q_R , the disturbance causes a new state for the agent. This actual state S_a is compared to the desired state at node ②. The difference of the two, measured by sensory inputs, leads to an error signal termed the control error (E):

$$E = S_d - S_a \quad (1)$$

This drives the reflex mechanism H_R to generate an action A_R which, by design, corrects for the disturbance and resumes equilibrium at node ①; this is the reflex action. The fixed controller is incapable of disturbance avoidance. For this reason, it is enclosed within the outer predictive loop whose task is to combat the disturbance D before it reaches the reflex loop and, thus, maintain the desired state S_d at all times.

2.2 The predictive loop

Contrary to the reflex, sign and relevance (SaR) network acts in anticipation and with prior knowledge of the disturbance. The purpose of the SaR is to perform without invoking the reflex pathway. The disturbance is first received by the predictive environment Q_P and is translated into predictive sensory inputs $[P]$. Based on this input information, the network generates a predictive action A_P in an attempt to resume, or preserve, system equilibrium at node ①, where the effects of A_P , the delayed D , and the reflex action A_R are combined before travelling through to the reflex loop. If successful, A_P fends off the delayed D precisely to yield a zero sum at this node¹ and thus, the reflex loop is not evoked. If unsuccessful, however, the summation yields a non-zero signal which is received by Q_R ; this evokes the reflex loop and leads to a non-zero control error signal.

2.3 The control error (E)

The function of the control error is two-fold: 1) it is received by the reflex H_R to generate the reflex action A_R , as described above, and 2) it serves as an instructive feedback for the learner. Through iterations, the non-zero E signal tunes the internal parameters of the SaR network. The learning terminates when A_P fends off the disturbance at node ③ precisely and persistently. In this case, the reflex loop is no longer evoked, E remains at zero, the learner undergoes no further changes, and thus, the SaR network has successfully generated the forward model of the reflex, in a similar fashion to the model-based learning paradigms presented in the work by [Porr and Wörgötter \(2002, 2006, 2003\)](#).

¹note that A_R is zero at this instance.

2.4 The SaR learner

The learner generates the forward model of the reflex through the mapping of its predictive actions onto a set of sensory consequences which is realised by the agent — the control error signal. The unique property of the SaR paradigm is that the instructive feedback of E is facilitated through two distinct pathways: 1) the backpropagation of the *sign* of E (green traces), and 2) global intervention of the rectified E (blue traces); refer to Figure 1.

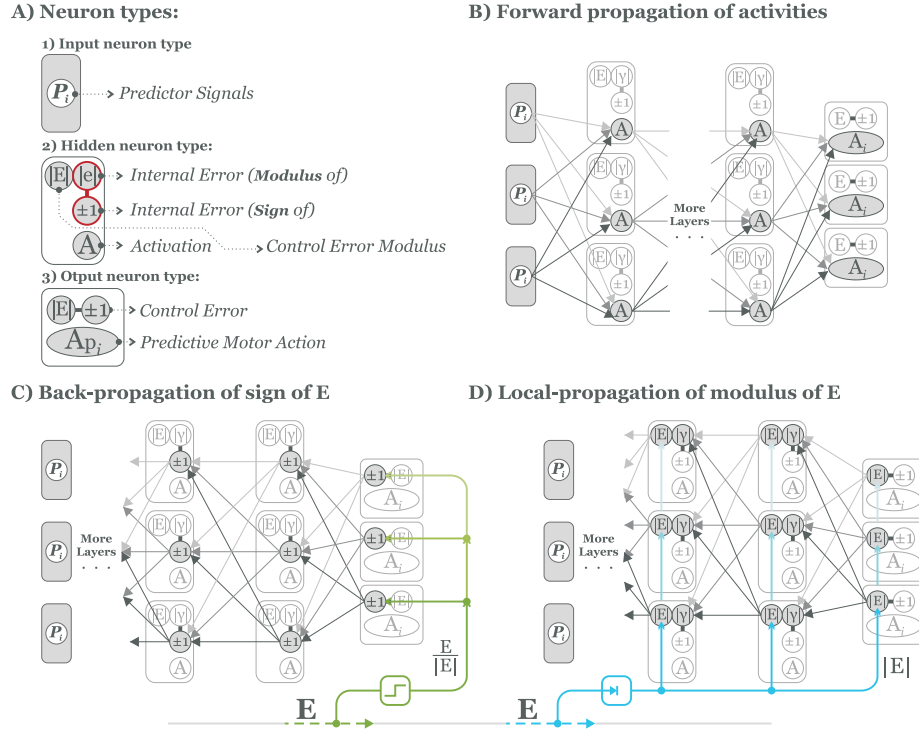


Figure 2: Signal pathways within SaR network A) Symbol introduction: 1) an input neuron, 2) a hidden neuron, and 3) an output neuron. B) The forward propagation of predictive signals, calculation of activations, and formation of motor commands. C) The backpropagation of the sign of E . D) The global injection and local propagation of E .

Figure 2 illustrates the three signal pathways within the SaR network. The symbols used for each neuron types are introduced in Figure 2A. The SaR learner employs a feed-forward neural network with fully connected layers. Figure 2B shows the forward pass of signals from the predictive inputs P_i , to activations A in deeper layers.

Figure 2C shows the back propagation of sign of E . The green traces mark the entry of E from the reflex loop onto the output neurons. The sign of E is propagated from the final layer to the deeper layers. Within each layer the sign of the resulting

value is used for propagation to the deeper layers. This results in a value of ± 1 within each neuron which primes their connections to be strengthened (+1) or weakened (-1). This is analogous to LTP and LTD in the context of neurophysiology.

Figure 2D shows the local propagation of the modulus of the E . The blue traces show the entry of this signal from the closed-loop platform onto every layer. This value is innervates each neuron and is propagated to the adjacent deeper layer only. The absolute value of the resulting sum dictates the amount by which the previously primed connections are strengthened or weakened. This is analogous to the effect of neuromodulators, in particular serotonin, on plasticity.

3 Mathematical derivation of sign and relevance (SaR) learning

In this section we derive the learning rule for sign and relevance (SaR) learning. First, forward propagation of predictive inputs to generation of the predictive action is derived as in the conventional flow of signals in fully connected feed-forward neural networks. Next, a mathematical expression of the learning goal in its general sense is presented where a differentiable function is optimised through adjustment of weights. Subsequently, this learning goal is unravelled with regards to the close-loop platform as well as the inner working of the neural network. With that, the learning rule for a conventional gradient descent method (GDM) is derived which leads to the formulation of the SaR update rule.

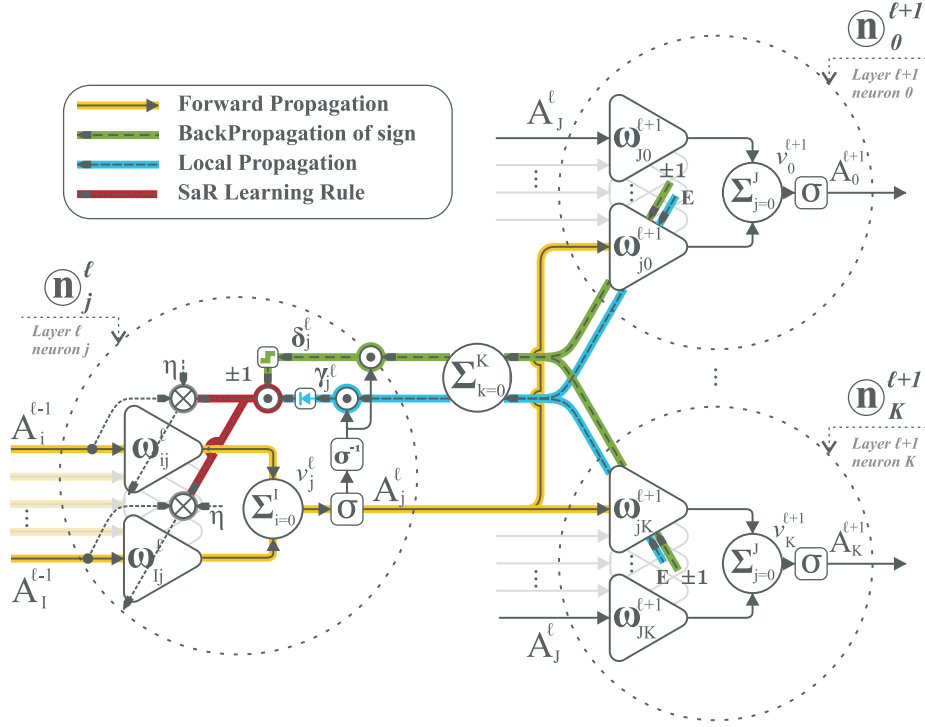


Figure 3: Inner connections of neurons in a sign and relevance (SaR) network. Yellow arrows present the forward pass of the activations, green arrows show the back propagation of sing of E , blue arrows display local propagation of the modulus of error, and red arrows highlight the learning.

3.1 Forward propagation of activations

Figure 3 demonstrates the inner mechanism of neurons and their connections. The forward propagation of activations, from j^{th} neuron in ℓ^{th} layer: \textcircled{n}_j^ℓ to all neurons in the adjacent deeper layer: $\textcircled{n}_{0 \rightarrow K}^{\ell+1}$, is highlighted by yellow solid lines. Equations 2 and 3 summarise the forward pass from the input layer, to hidden layers, and to the output layer:

$$[A]^1 = \sigma([v]^1) = \sigma([\omega]^1 \odot [P]) \quad \text{Input layer} \quad (2)$$

$$[A]^\ell = \sigma([v]^\ell) = \sigma([\omega]^\ell \odot [A]^{\ell-1}) \quad \text{Hidden layers} \quad (3)$$

where A^x , v^x and ω^x denote the activation, sum-output, and the weight matrices within the x^{th} layer, respectively. A linear function of output activations forms the predictive

action $A_P = f([A]^L)$. As described in section 2, upon execution of the predictive action, a series of events take place in the closed-loop platform that leads to the generation of E , defined in Eq. 1; this signal governs the learning of the SaR network.

3.2 The learning goal

The learning goal is to actively and consistently keep the control error at zero; this is achieved through adjusting the weight matrices $[\omega]^x$. From a mathematical stand point, the learning objective is best formulated as an optimisation task, where the quadratic of the control error is minimised with respect to the weights:

$$[\omega]^{1 \rightarrow L} = \arg \min_{[\omega]} E^2 \quad (4)$$

In other words, we seek weight matrices for all layers $[\omega]^{1 \rightarrow L}$ such that the generated A_P minimises E^2 ; this is analogous to forcing E towards zero. When faced with an optimisation task, a widely employed practice is that of the gradient descent method (GDM), where the adjustment to an arbitrary weight is proportional to the sensitivity of E^2 with respect to the sum-output of the neuron associated with that weight:

$$\Delta[\omega]^\ell = \frac{\partial E^2}{\partial [v]^\ell} \odot \frac{\partial [v]^\ell}{\partial [\omega]^\ell} \quad (5)$$

Referring to Equation 3, the later gradient yields the matrix of activation inputs to the neuron: $[A]^{\ell-1}$. The former gradient, however, relates a closed-loop signal (E) to an internal parameter of the network (v). The linking entity between the closed-loop platform and the neural network is the predictive action A_P (Daryanavard and Porr, 2020), and thus, by applying the chain rule, the closed-loop signals are separated from the internal parameters of the network:

$$\frac{\partial E^2}{\partial [v]^\ell} = \frac{\partial E^2}{\partial A_P} \cdot \frac{\partial A_P}{\partial [v]^\ell} \quad (6)$$

3.3 Dynamics of the closed-loop platform

We seek an expression that relates the control error (E) to the predictive output A_P . In Equation 1, substituting for S_a results in:

$$\begin{aligned} E &= S_d - Q_R \overbrace{(A_R + A_P + Dz^{-T})}^{\text{Figure 1, node ①}} \\ &= S_d - Q_R(EH_R + A_P + Dz^{-T}) \\ &= \frac{S_d - Q_R(A_P + Dz^{-T})}{1 + Q_R H_R} \end{aligned} \quad (7)$$

Therefore:

$$\kappa = \frac{\partial E^2}{\partial A_P} = 2E \frac{\partial E}{\partial A_P} = 2E \frac{-Q_R}{1 + Q_R H_R} \quad (8)$$

where $\frac{-Q_R}{1+Q_R H_R}$ is the reflex loop gain and is measured experimentally. This partial gradient is referred to as the closed-loop gradient and is denoted by κ .

3.4 Inner dynamics of the neural network

We seek an expression that related the predictive output A_P to the matrix of sum-outputs $[v]^\ell$ in an arbitrary layer. To that end, Equation 3 can be rewritten as below:

$$\sigma([v]^{\ell+1}) = \sigma([\omega]^{\ell+1} \odot \sigma([v]^\ell)) \quad (9)$$

Differentiation of A_P with respect to $[v]^\ell$ yields:

$$[\delta]_{GDM}^\ell = \frac{\partial A_P}{\partial [v]^\ell} = \sigma^{-1}([v]^\ell) \odot ([\omega]^{\ell+1T} \odot \frac{\partial A_P}{\partial [v]^{\ell+1}}) \quad (10)$$

This partial gradient is referred to as the internal error and is denoted by matrix $[\delta]^\ell$; note the recursive nature of this operation, where calculation of this partial gradient in the ℓ^{th} layer depends on the value of this gradient in the $(\ell + 1)^{th}$ layer. Therefore, starting from the final layer, let f be the function that generates the predictive output given the activation matrix of the output layer:

$$A_P = f(\sigma([v]^L)) \quad (11)$$

Differentiation with respect to the sum-output matrix v^L yields:

$$[\delta]^L = \frac{\partial A_P}{\partial [v]^L} = f^{-1}(\sigma([v]^L)) \cdot \sigma^{-1}([v]^L) \quad (12)$$

Calculation of this gradient in the final layer and using the backpropagation (BP) technique resolves the internal errors for all layers.

3.5 The gradient descent method (GDM) learning rule

Finally, the learning rule using the gradient decent method is given as:

$$\Delta_{GDM}[\omega]^\ell = \kappa \cdot \eta \cdot ([\delta]^\ell \odot [A]^{\ell-1}) \quad (13)$$

where η is the learning rate. As explained in the introduction section, this learning can suffer from exploding and vanishing gradient problem (EVGP), and is reliant on weight symmetry which is shown to be biologically implausible. In the following section we derive the SaR learning rule which is free from EVGP and is a stronger candidate for learning in the context of neuroscience.

3.6 The sign and relevance (SaR) learning rule

In this work, merely the *sign* of the internal error $[\delta]^\ell$ is used for backpropagation into deeper layers. The green dashed arrows in Figure 3 highlight the propagation of signs. The result of this propagation is a matrix of signs² for each layer represented as: $[\pm 1]^\ell$. This matrix is calculated by a throughout propagation and, in this manner, carries information about the *network-wide* connections of the neurons:

$$[\pm 1]^\ell = \frac{[\delta]^\ell}{|[\delta]^\ell|} = \frac{\sigma^{-1}([v]^\ell) \odot ([\omega]^{\ell+1T} \odot [\pm 1]^{\ell+1})}{|\sigma^{-1}([v]^\ell) \odot ([\omega]^{\ell+1T} \odot [\pm 1]^{\ell+1})|} \quad (14)$$

The magnitude of the weight change, however, is derived from a local propagation of E , and thus, it provides insight about the *one-layer-deep* connections of the neurons, as well as being directly influenced by the control error. The local propagation of error is shown by blue dashed arrows in Figure 3 and is formulated as:

$$[\gamma]^\ell = \sigma^{-1}([v]^\ell) \odot ([\omega]^{\ell+1T} \cdot E) \quad (15)$$

where $[\gamma]^\ell$ is the matrix of local errors in the ℓ^{th} layer. For the final layer we have:

$$[\gamma]^L = f^{-1}(\sigma([v]^L)) \odot \sigma^{-1}([v]^L) \cdot E \quad (16)$$

with that, the learning rule for the SaR network is defined as:

$$\Delta[\omega]_{\text{SaR}}^\ell = \kappa \cdot \eta \cdot (([\pm 1]^\ell \odot |[\gamma]^\ell|) \odot [A]^\ell)^{-1} \quad (17)$$

4 Implementation of SaR learning on a navigational robot

The learning algorithm presented in this work is implemented on a path-following robot — the organism, with the task of navigating a canvas whilst retaining a symmetrical positioning on a path printed on the canvas — the environment; see Figure 4C.

4.1 The robotic platform

Schematic drawings of the robot are shown in Figure 4A and 4B respectively (not to scale). The chassis of the robot houses a battery and contains the wiring of the components. The robot consists of two wheels, an array of light sensors and a camera. The camera provides a vision of the path ahead in the form of a matrix. A Raspberry Pi 3B+ (RPi) with remote connection is used as a processing centre that hosts the algorithm. In the following subsections, both reflex and predictive sensory inputs as well

²This matrix only contains values of +1, -1 or 0.

as the motor command are described and the components of the robot are discussed in depth.

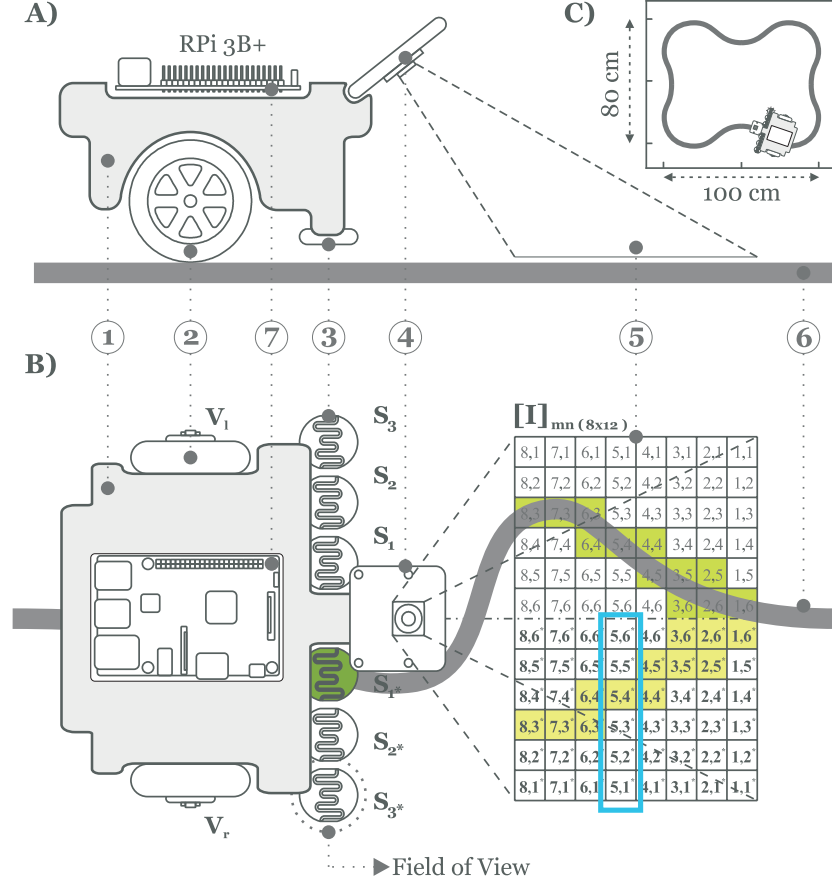


Figure 4: Schematics of the robot (not to scale): A) Side view B) Top view; showing the chassis ①, the wheels ②, an array of six light dependent resistors (LDRs) ③, the camera ④, the predictive matrix ⑤, the path ⑥, a Raspberry Pi 3B+ (RPi) ⑦. C) The canvas and the path.

4.2 Reflex sensory inputs

The light array consists of 6 symmetrically positioned light dependent resistors (LDRs) which are placed underneath the chassis in close proximity of the canvas as in Figure 4A, labelled $S_{1,2,3}$ on the left and $S_{1^*,2^*,3^*}$ on the right³ side of the robot in Figure 4B. Each sensor receives the reflected light from a small portion of the canvas

³Star sign indicates the symmetrical positioning of an arbitrary sensor with respect to its unmarked counterpart

directly underneath. This region is referred to as the field of view (FoV) of the sensor, indicated by a dotted circle around sensor S_{3^*} in Figure 4B. During navigation, these sensors translate the changes in the intensity of the reflected light into voltage fluctuations. As the FoV of a sensor transitions from capturing the black path entirely to capturing the white background, it generates a voltage potential within the range of $600 - 1500[mV]$. The ground (G) value, G_i or G_{i^*} , of each sensor is found through a linear mapping of their voltage potentials to the range $[0, 256) \in \mathbb{N}$ so as to represent the gray-scale value (GSV) of their respective FoVs. The G value of each sensor is proportional to the presence of the black path in their FoV which provides a measure of the vertical alignment of the sensor with respect to the path and thus serves as an indicator for the relative positioning of the robot. For example, sensor S_{1^*} in Figure 4B is vertically aligned with the path indicating a slight deviation of the robot to the right, whereas, alignment of sensor S_3 would indicate a significant deviation to the left.

In technical terms, the deviation of the robot from the path is measured through a weighted sum of differences in G values of sensor pairs. Thus, the experimental value of the control error (E), previously defined in Equation 1, is found as:

$$E = \sum_{i=1}^3 K_i (G_i - G_{i^*}) \quad [\text{GSV}] \quad (18)$$

where K_i is a weighting factor whose magnitude increases linearly with i , so as to reflect the degree of deviation. Meaning, the farther the active sensor from the centre line the greater the spike in E , indicating a greater deviation.

4.3 Predictive sensory inputs:

the camera provides information about the path in the near distance and thus facilitates anticipatory steering of the robot. The camera captures a 1280 by 720 pixel image which is segmented into regions as in Figure 4B. Each square region is assigned the average GSVs of the pixels it contains. This generates the sensory input from the camera in the form of a 8 by 12 matrix $[I]_{mn}$. Similar to that of the light array sensors, the difference of symmetrical entries in this matrix measures the anticipated degree of deviation in the near distance:

$$C_{ij} = I_{ij} - I_{ij^*} \quad \text{where} \quad 1 \leq i \leq m, \quad 1 \leq j \leq \lfloor \frac{n}{2} \rfloor \quad \text{and} \quad j^* + j = n + 1 \quad (19)$$

Where C_{ij} are difference signals that form an 8 by 6 matrix. A non-zero C_{ij} indicates an upcoming turn; the value of j indicates the sharpness of the turn, whilst the value of i indicates the distance of the turn from the current position, and the sign of C_{ij} indicates a right or left turn. Each difference signal is delayed using a filter array (FA) of 5 finite impulse response (FIR) filters, F_h , so as to observe an optimum correlation with the control error signal during for learning (Daryanavard and Porr, 2020):

$$P_k = F_h * C_{ij} \quad (20)$$

where $1 \leq h \leq 5, \quad 1 \leq i \leq m, \quad 1 \leq j \leq \lfloor \frac{n}{2} \rfloor$

This results in a sequence of 240 predictor signals P_k which are fed into the neural network for prediction and producing anticipatory action.

4.4 The motor command (MC)

The navigation of the robot is facilitated through adjustments to the speeds of the right and left wheels, V_R and V_L , that otherwise proceed forward with a fixed speed of $V_0 = 5[\frac{cm}{s}]$. A motor command (MC) is sent to the wheels that modifies the velocities of each wheel as:

$$\begin{cases} V_R = V_0 + MC, & \text{for right wheel.} \\ V_L = V_0 - MC, & \text{for left wheel.} \end{cases} \quad (21)$$

MC is generated jointly by both the reflex and predictive mechanism of the robot and hence is the sum of reflex and predictive actions introduced in Section 2:

$$MC = A_R + A_P \quad (22)$$

where A_R is proportional to E and A_P is a weighted sum of the activations in the output layer as indicated in Equation 11:

$$\begin{cases} A_R \propto E, & \text{reflex action.} \\ A_P = f([A]^L) = [M] \odot [A]^L, & \text{predictive action.} \end{cases} \quad (23)$$

where $[M]$ is a weighting matrix for output activations; this facilitates sharp, moderate, or slow steering of the robot depending on the active neuron and its weighting. At initial stages of a trial, A_R is the main contributor to the motor command, as the learning progresses A_P delivers a more adequate contribution, and upon successful learning, where the SaR network has generated the forward model of the reflex, A_R is kept at zero at all times and A_P alone controls the motor command.

4.5 Architecture of the sign and relevance (SaR) network

This application employs a feed forward neural network with fully connected layers. As derived in Equation 20, there are 240 inputs from the camera, and thus, the network is initialised with 240 neurons in the input layer. The number of neurons in the hidden layers decrements linearly from 13 to 4 through 10 hidden layers. Finally, there are 3 neurons in the output layer and the weighted sum of their activations, using $[M] = [1, 3, 5]$, yields the predictive action as in Equation 23 where .

5 Results

In this section we present a comparison between the conventional GDM technique and SaR learning. For completion, we also present an additional set of results using only locally propagated relevance signal, so as to better signify the importance of simultaneous backpropagation of sign and local propagation of the relevance components of the E signal in SaR paradigm. We define the local propagation learning rule as:

$$\Delta[\omega]_{Local-Prop}^\ell = \kappa \cdot \eta \cdot ([\gamma]^\ell \odot [A]^{\ell-1}) \quad (24)$$

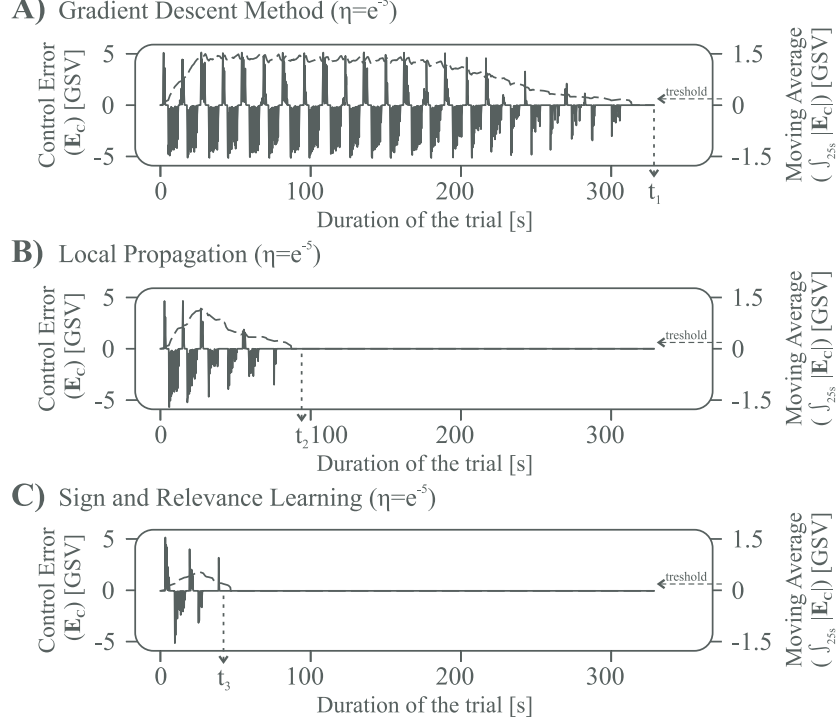


Figure 5: The control error (E) signal and it's 25[s] moving average during learning trials with conventional GDM (A), local propagation (B), and SaR learning (C) with the learning rate of $\eta = e^{-5}$.

Figure 5 shows a set of trials with learning rate of $\eta = e^{-5}$. Sections A, B and C of this figure show the control error (E) signal (solid traces) and its absolute moving average over 25 seconds: $\bar{E} = \int_t^{t-25} |E(t)|$ (dashed traces) for the three learning modalities mentioned above. We define *success* as a state where \bar{E} falls below a value of 0.1[GSV] (left-hand-side axes); this is evaluated 12 seconds after the trial has commenced to allow for the signal to accumulate.

During a trial with GDM, the error signal is persistent for approximately 200 seconds before it gradually converges reaching the success state at time $t_1 = 333$ [s]. This trial sets a benchmark for evaluation of the two later learning modalities. Section B shows these results for a learning trial with local propagation only. This trial shows a much faster learning than that of the GDM technique, where the error signal is persistent for only 20 seconds before it converges to the success state at time $t_2 = 93$ [s]. Lastly, section C shows these results for a trial with SaR learning, where the BP of the sign of the error, and the magnitude of the locally propagated error, join to drive the the weight changes. It can be seen that the learning is significantly improved, in that, the error signal does not persist, rather, it immediately begins to converge and successful learning is achieved at time $t_3 = 42$ [s].

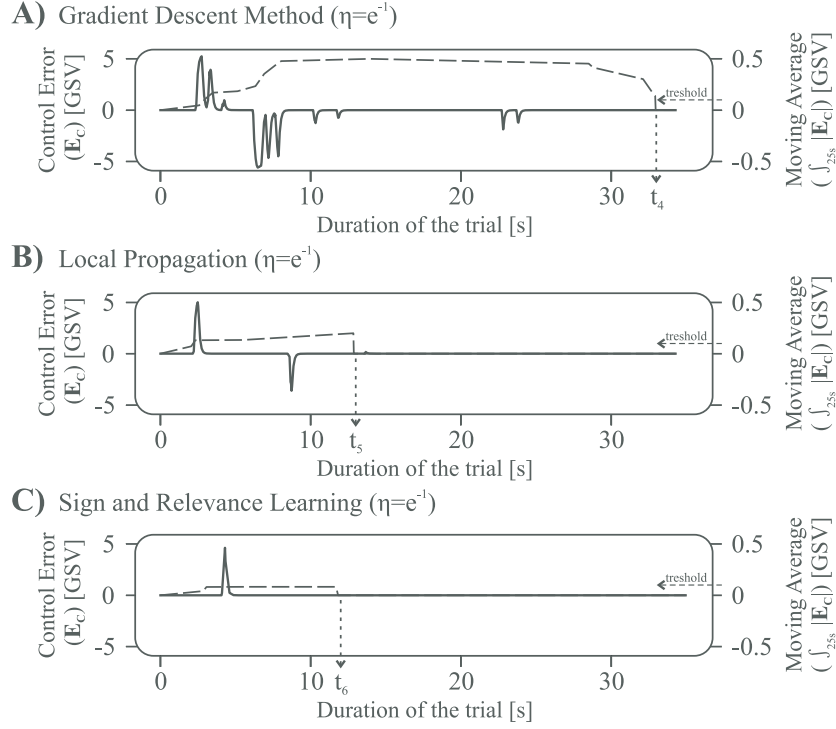


Figure 6: The control error (E) signal and it's 25[s] moving average during learning trials with conventional GDM (A), local propagation (B), and SaR learning (C) with the learning rate of $\eta = e^{-1}$.

Figure 6 shows another set of trials with a faster learning rate of $\eta = e^{-1}$. In section A, during a trial with GDM, the error signal spikes over a period of 25[s] before it fully converges at $t_4 = 32[s]$. In section B, during a trial with local propagation only, the error signal only spikes twice before it fully converges at $t_5 = 13[s]$. At last, in section C, *one-shot* learning is achieved during a trial with SaR; the error signal spikes once at $t = 5[s]$ and the success state is achieved at $t = 12[s]$. It can be seen that in the two former trials the moving average remains below the success threshold, therefore total integral of the error during these trials is a better comparative factor.

Additional information about one-shot learning with SaR is presented in Figure 7. Sections A, B and C show the control error signal, the activity of six selected predictive signals marked with blue rectangle in Figure 4B, and the predictive action A_P , respectively. The robot first encounters the line at time $t_7 = 8[s]$. Prior to this instant, some predictive signals are active, however, there is no steering signal at the output of the network ($A_P = 0$)⁴. Upon encountering the line, the control error spikes. This signal generates the reflex reaction so as to return the robot to the path, and trains the neural network in order to produce adequate steering signal. Hence the error signal returns to

⁴This is due to the fact that the robot is initially positioned on the path symmetrically.

zero at $t_8 = 9[s]$. The gradual increase in the output of the network from t_7 to t_8 , in section C, signifies the learning driven by the non-zero error signal during this interval. Subsequent to this learning, the predictive signals provide the network with clues about the path ahead and the neural network produces adequate predictive action, as a result, the error signal remains at zero for the remainder of the trial.

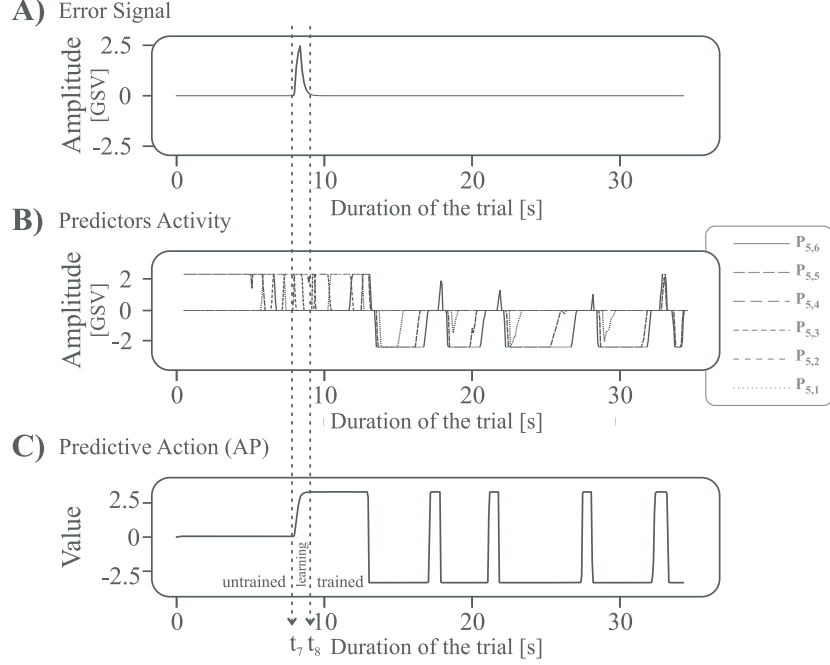


Figure 7: The control error (E) signal (A), the activity of six selected predictive signals (B), and the output of the neural network (C) during a learning trial with SaR learning with the learning rate of $\eta = e^{-1}$.

Naturally, one-shot learning in the context of deep learning begs the question of weight stability. In this work the euclidean distance of weights in each layer is used as an indicator of weight convergence stability. This is calculated as the multidimensional distance of the weight matrix $[\omega]$ at time t' from its initialisation matrix at time t_0 :

$$Ed(t') = euclidean([\omega]_{t'}, [\omega]_{init}) = \sqrt[2]{\sum_{i,j=0}^{I,J} (\omega_{ij}^{\ell}|_{t'} - \omega_{ij}^{\ell}|_{t_0})^2} \quad (25)$$

This parameter is calculated within individual layers of the network where ℓ is constant.

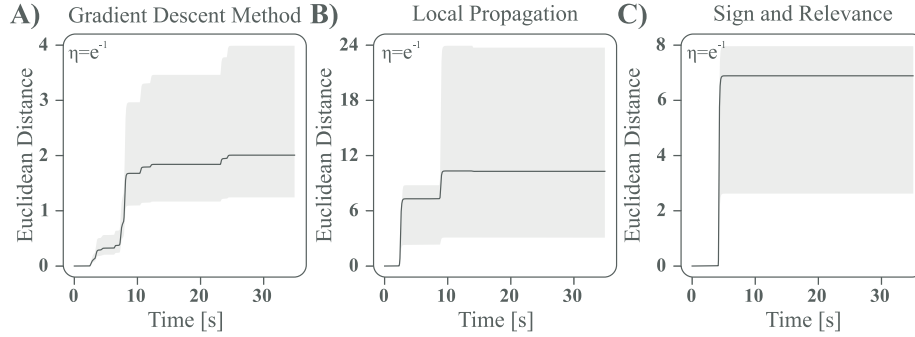


Figure 8: The euclidean distance of weights in the first layer (black traces) and in deeper layers (grey shadow) during learning trials with conventional GDM (A), local propagation (B), and SaR learning (C) with the learning rate of $\eta = e^{-1}$.

Figure 8 shows the euclidean distance of weights during the three trials previously produced in Figure 5. Section A shows that in a trial with GDM, the final euclidean distance of weights in deeper layers fall within a range of 1.2 to 4 (the grey area). However, the changes in the first layer, where the sensory consequences of motor actions are perceived, carry more significance (Porr and Miller, 2020). Therefore, euclidean distance of the first layer is shown individually by the black trace with a final distance of ≈ 2 for this trial. This is used as a reference for investigating the nature of weight changes for other learning paradigms.

As for the trial with local propagation, the final euclidean distance for deeper layers range from 3 to 24, with the first layer showing a distance of ≈ 10 . This is a significant increase from that of GDM. However, section C shows this result for a trial with SaR learning where the euclidean distance is moderately greater than that of the GDM, with final distance of 3 to 8 for deeper layers and ≈ 7 for the first layer. Though, the euclidean distance has almost doubled, it has done so whilst improving the speed and the performance of the SaR learner. On the contrary, the significant weight change observed in the trial with local propagation offers no further improvement to that obtained with SaR learning. This raises uncertainty about the nature of convergence and stability of the network with local propagation only. This result homes in on the fact that the local propagation is not solely responsible for the outstanding performance of the SaR learner, whereas, the sign backpropagation of the error signal is the principal factor in ensuring a fast but stable learning network-wide.

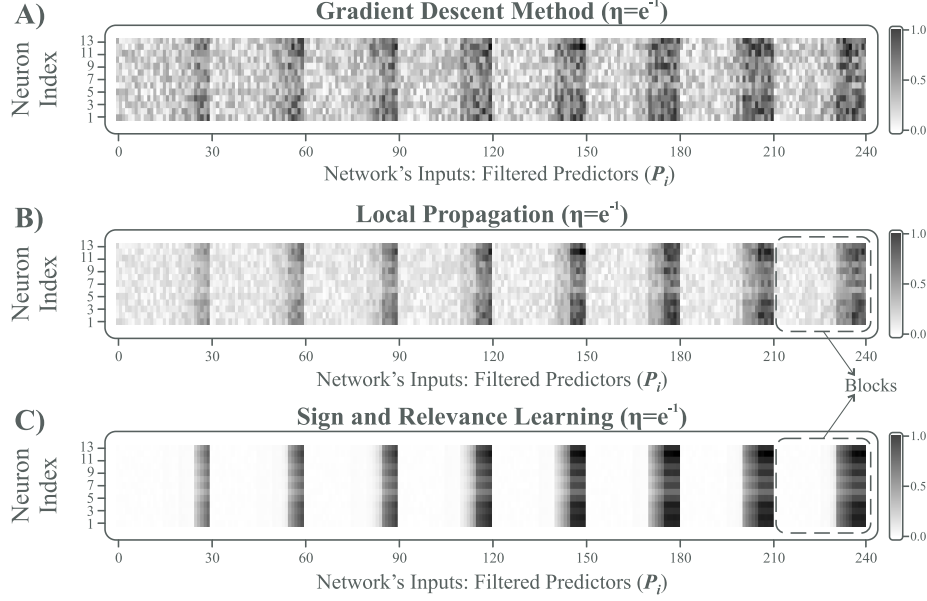


Figure 9: *Final weight distributions in the first hidden layer during learning trials with conventional GDM (A), local propagation (B), and SaR learning (C) with the learning rate of $\eta = e^{-1}$.*

As mentioned above, there is a greater significance associated with the first hidden layer where the organism learns to assign importance to the sensory inputs received from the environment. Figure 9 displays the final weight distributions in the first hidden layer for the trials previously discussed in Figures 5 and 8. There are 240 predictive input signals and 13 neurons in the first hidden layer, making a 240 by 13 matrix of weights. The values in this matrix are normalised to $[0, 1]$ and are assigned shades of grey, white corresponding to 0 and to black to 1, creating an image of weight distribution. Common observations amongst the three learning paradigms are: 1) the 8 rows of predictors (see Figure 4) are appropriately classified into recognisable blocks, 2) within each block there is a gradient where outermost columns of predictors (see Figure 4) are assigned a higher value producing a sharper steering and, 3) this gradient is more predominant for rows of predictors closer to the robot (rightmost blocks). However, a comparison of the trials reveals a more assured and well defined gradient for SaR learning (C) than local propagation (B) and that of the GDM (A).

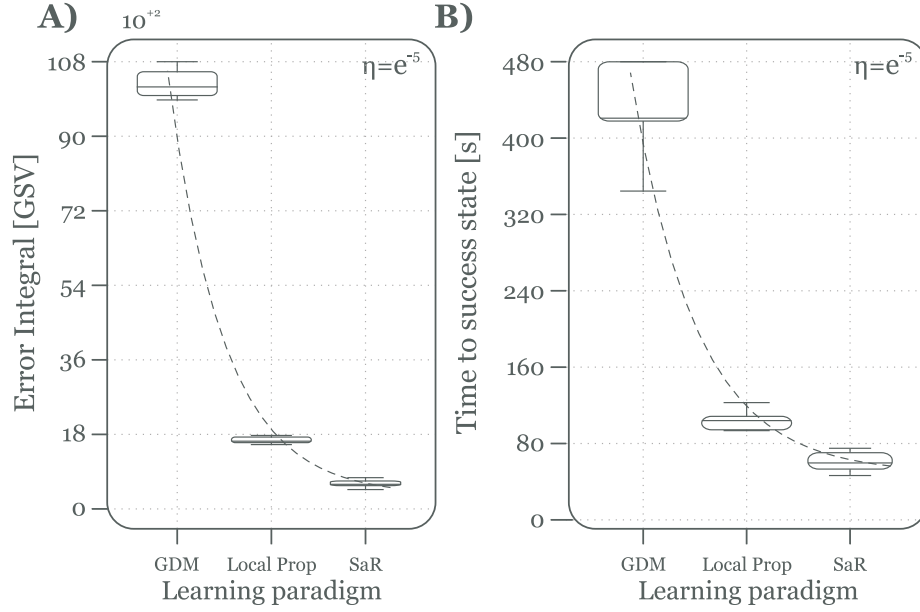


Figure 10: *Reproducibility of results showing total error integral (A) and time taken to success state (B) for 10 trials with GDM, local propagation and, SaR learning.*

The trials presented in Figure 5 were repeated 10 times to demonstrate the reproducibility of the results. Figure 10 A and B display the total error integral and the time taken to reach the success state for trials with GDM, local propagation and SaR learning. In support of the results produced in Figure 5, it can be concluded that SaR consistently provides a faster learning with smaller error accumulation. Additional trials were carried out with local propagation and SaR with learning rates of $\eta = \{e^{-5}, e^{-4}, e^{-3}, e^{-2}, e^{-1}\}$; Figure 11 shows the result of these experiments. Conceivably, SaR learning performs faster with smaller error accumulation.

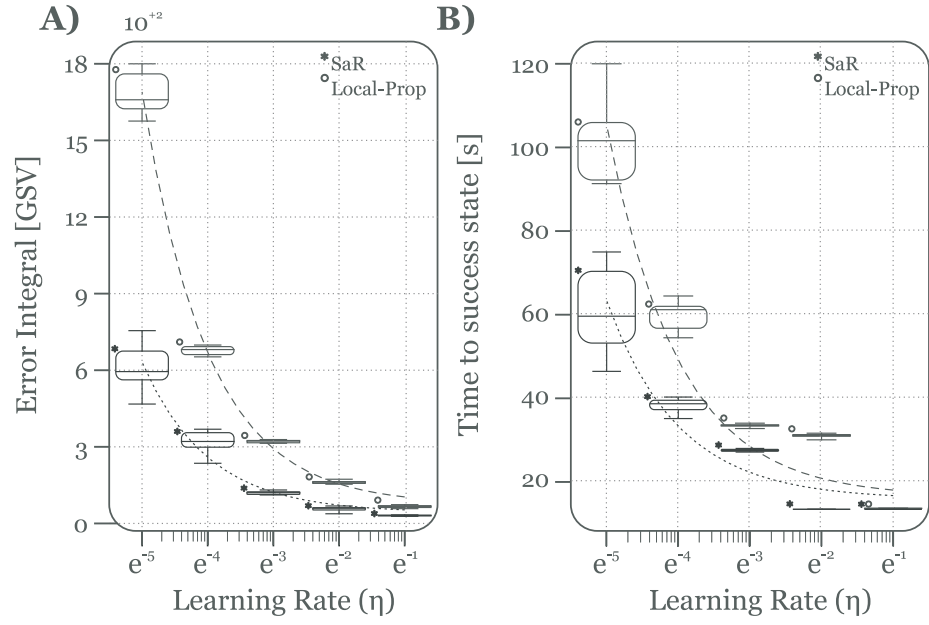


Figure 11: *Reproducibility of results with different learning rates showing total error integral (A) and time taken to success state (B) for trials with local propagation (dashed curve) and SaR (dotted curve).*

6 Discussion

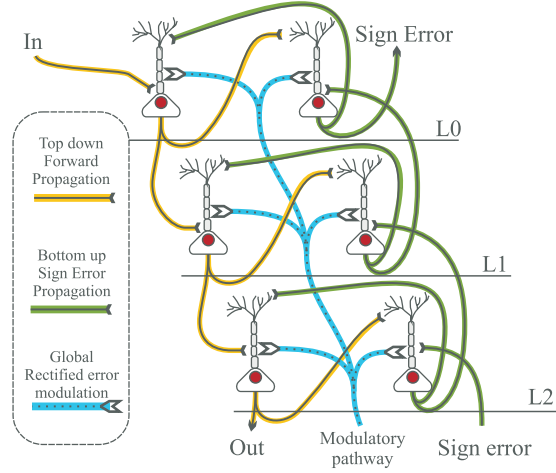


Figure 12: *Proposal of a neurophysiologically realistic model of SaR learning. Shown are three network layers L0-L2. Signal processing is performed in three pathways: “Top down” which transmits a signal from “In” to “Out”, a “Bottom up” pathway which transmits the Sign error and a “Modulatory pathway” which provides a global signal to all neurons. The top down and bottom up pathways transmit signals via synapses close to the respective somas while the reciprocal connections between the neurons within a layer connect to the dendrites influencing plasticity.*

In this paper we presented a learning algorithm that separates the error signal into a global and local component where only its sign is backpropagated through the network while its rectified value is transmitted globally to all layers. In contrast to classical backpropagation, this approach is significantly faster in a closed loop learning task and complies with neurophysiology more closely by employing both neuromodulators and local learning rules while not requiring strictly symmetric weights.

Deep learning has become very popular over the last decade (Guo et al, 2014) and given that it uses neural networks it should also be a good candidate to explain how the brain itself conducts learning (Marblestone et al, 2016). For example, Lillicrap et al (2016b) maps deep learning on the brain, however, due to the neurophysiologically unrealistic requirement of symmetric weights between forward and backward pathways

this is limited to few layers.

On the other hand, traditional biologically realistic reinforcement learning models (Schultz and Suri, 2001; Wörgötter and Porr, 2005; Prescott et al, 2006) employ the reward prediction error which has a strong familiarity to the dopaminergic signal in the striatum (Schultz et al, 1997). These models are certainly closer to biology but suffer from the problem that any global error signal poses for deep structures namely, the different layers change all similarly and therefore a deep structure adds little to their performance.

However, do reward related neuromodulators convey error signals as it has been the dominant paradigm during the last two decades Schultz et al (1997)? Serotonin appears to rather code reward expectation (Li et al, 2016) which could at best be called a “rectified” reward prediction error. Similarly, the negative response of dopamine neurons to a negative reward expectation has been declared as unreliable by Schultz (2004) due to its low baseline firing rate of approximately 1 Hz, resulting in a very low signal to noise ratio. A different interpretation for both the serotonin and also the dopamine signal is that of a relevance signal (Porr and Wörgötter, 2007) ramping up or enabling plasticity (Loving, 2010; Iigaya et al, 2018) while local plasticity learning rules determine if synaptic weights undergo long-term potentiation (LTP) or long-term depression (LTD) (Castellani et al, 2001; Inglebert et al, 2020).

Given that we have established global and local learning we can now discuss how such processing can be established in the brain. Fig. 12 shows the suggested circuit inspired by Larkum (2013); Rolls (2016) and with added neuromodulatory innervation (Loving, 2010; Iigaya et al, 2018). This circuit has two distinct pathways where the top-down pathway carries, for example, sensor signals to deeper structures of the brain or directly to motor outputs. As an example, a single top-down path is depicted from “In” to “Out” via three synapses connecting the three neurons in layer zero to layer two. Having described the top-down path we can now look at the bottom-up path. It transmits the sign of the error signal from layer two back to layer zero; this pathway also has three synapses. Finally, we can now look at the global neuromodulation which controls the plasticity at all neurons which leads us to the plasticity rules. Central to this circuit is that the local plasticity is driven by the concentration of postsynaptic Calcium. Following the reasoning of Inglebert et al (2020) only a strong Calcium influx caused by both somatic burst spiking and dendritic Calcium spikes will lead to long-term potentiation (LTP) while less activity, in particular lack of dendritic Calcium bursts, will lead to long-term depression (LTD). Projections from the distal parts to the dendrite are not able to make the neuron spike, however, if coincident with a somatic input, it will create long lasting bursting causing LTP (Larkum, 2013) owing to a large influx of Calcium (Inglebert et al, 2020). Conversely, if the dendritic trees are not sufficiently driven, LTD will be initiated due to a smaller Calcium influx from single spikes (Inglebert et al, 2020; Shouval et al, 2002). Thus, the *sign* of the weight development between reciprocal neurons within a layer in both top-down and bottom-up pathways is mirrored due to their reciprocal connections and their ability to boost or deprive each other’s Calcium concentrations. The neuromodulator then controls the actual plasticity, meaning that the requirement of symmetric weights within a layer is relaxed and is replaced by the requirement that the weights undergo either LTP or LTD, whilst the rate of weight change is determined by the neuromodulator. Future research is needed to

investigate this model in depth using more detailed biophysical models, in the hope of showing that not only do these models bring deep learning closer to neurophysiology but also they carry positive implications for mental illness models (Rolls, 2016).

References

- Bengio Y, Simard P, Frasconi P (1994) Learning long-term dependencies with gradient descent is difficult. *IEEE transactions on neural networks* 5(2):157–166
- Berthoud H (2004) Mind versus metabolism in the control of food intake and energy balance. *Physiol Behav* 81(5):781–793
- Bliss T, Lomo T (1973) Long-lasting potentiation of synaptic transmission in the dentate area of the anaesthetized rabbit following stimulation of the perforant path. *J Physiol* 232(2):331–356
- Bromberg-Martin ES, Matsumoto M, Hikosaka O (2010) Dopamine in motivational control: rewarding, aversive, and alerting. *Neuron* 68(5):815–34, DOI 10.1016/j.neuron.2010.11.022
- Castellani GC, Quinlan EM, Cooper LN, Shouval HZ (2001) A biophysical model of bidirectional synaptic plasticity: Dependence on AMPA and NMDA receptors. *Proc Natl Acad Sci (USA)* 98(22):12,772–12,777
- Daryanavard S, Porr B (2020) Closed-loop deep learning: Generating forward models with backpropagation. *Neural Computation* 32(11):2122–2144
- Dayan P, Balleine BW (2002) Reward, motivation, and reinforcement learning. *Neuron* 36(2):285–298
- Guo X, Singh S, Lee H, Lewis RL, Wang X (2014) Deep learning for real-time atari game play using offline monte-carlo tree search planning. In: Ghahramani Z, Welling M, Cortes C, Lawrence ND, Weinberger KQ (eds) *Advances in Neural Information Processing Systems 27*, Curran Associates, Inc., pp 3338–3346
- Haber S, Kunishio K, Mizobuchi M, Lynd-Balta E (1995) The orbital and medial prefrontal circuit through the primate basal ganglia. *J Neurosci* 15(7 Pt 1):4851–4867
- Hebb DO (1949) *The organization of behavior: A neuropsychological study*. Wiley-Interscience, New York
- Humphries MD, Stewart RD, Gurney KN (2006) A physiologically plausible model of action selection and oscillatory activity in the basal ganglia. *Journal of Neuroscience* 26(50):12,921–12,942, DOI 10.1523/JNEUROSCI.3486-06.2006, URL <https://www.jneurosci.org/content/26/50/12921>, <https://www.jneurosci.org/content/26/50/12921.full.pdf>

- Iigaya K, Fonseca MS, Murakami M, Mainen ZF, Dayan P (2018) An effect of serotonergic stimulation on learning rates for rewards apparent after long intertrial intervals. *Nature Communications* 9(1):2477, DOI 10.1038/s41467-018-04840-2, URL <https://doi.org/10.1038/s41467-018-04840-2>
- Inglebert Y, Aljadeff J, Brunel N, Debanne D (2020) Synaptic plasticity rules with physiological calcium levels. *Proc Natl Acad Sci U S A* 117(52):33,639–33,648, DOI 10.1073/pnas.2013663117
- Larkum M (2013) A cellular mechanism for cortical associations: an organizing principle for the cerebral cortex. *Trends in neurosciences* 36(3):141–151
- Li Y, Zhong W, Wang D, Feng Q, Liu Z, Zhou J, Jia C, Hu F, Zeng J, Guo Q, Fu L, Luo M (2016) Serotonin neurons in the dorsal raphe nucleus encode reward signals. *Nature Communications* 7(1):10,503, DOI 10.1038/ncomms10503, URL <https://doi.org/10.1038/ncomms10503>
- Lillicrap TP, Cownden D, Tweed DB, Akerman CJ (2016a) Random synaptic feedback weights support error backpropagation for deep learning. *Nature communications* 7(1):1–10
- Lillicrap TP, Cownden D, Tweed DB, Akerman CJ (2016b) Random synaptic feedback weights support error backpropagation for deep learning. *Nature communications* 7:13,276, DOI 10.1038/ncomms13276
- Linley SB, Hoover WB, Vertes RP (2013) Pattern of distribution of serotonergic fibers to the orbitomedial and insular cortex in the rat. *Journal of chemical neuroanatomy* 48-49:29–45, DOI 10.1016/j.jchemneu.2012.12.006, URL <http://www.ncbi.nlm.nih.gov/pubmed/23337940>
- Lovinger DM (2010) Neurotransmitter roles in synaptic modulation, plasticity and learning in the dorsal striatum. *Neuropharmacology* 58(7):951–61, DOI 10.1016/j.neuropharm.2010.01.008
- Lu W, Man H, Ju W, Trimble WS, MacDonald JF, Wang YT (2001) Activation of synaptic NMDA receptors induces membrane insertion of new AMPA receptors and LTP in cultured hippocampal neurons. *Neuron* 29(1):243–54, DOI 10.1016/s0896-6273(01)00194-5
- Luo M, Zhou J, Liu Z (2015) Reward processing by the dorsal raphe nucleus: 5-HT and beyond. *Learn Mem* 22(9):452–60, DOI 10.1101/lm.037317.114
- Marblestone AH, Wayne G, Körding KP (2016) Toward an integration of deep learning and neuroscience. *Frontiers in computational neuroscience* 10:94
- Markram H, Lübke J, Frotscher M, Sakman B (1997) Regulation of synaptic efficacy by coincidence of postsynaptic apss and epsps. *Science* 275:213–215

- Mattson MP, Maudsley S, Martin B (2004) Bdnf and 5-HT: a dynamic duo in age-related neuronal plasticity and neurodegenerative disorders. *Trends in Neurosciences* 27(10):589–594, DOI <https://doi.org/10.1016/j.tins.2004.08.001>, URL <https://www.sciencedirect.com/science/article/pii/S0166223604002589>
- O'Reilly RC, Frank MJ (2006) Making Working Memory Work: A Computational Model of Learning in the Prefrontal Cortex and Basal Ganglia. *Neural Computation* 18(2):283–328, DOI 10.1162/089976606775093909, URL <https://doi.org/10.1162/089976606775093909>, <https://direct.mit.edu/neco/article-pdf/18/2/283/816470/089976606775093909.pdf>
- Pascanu R, Mikolov T, Bengio Y (2013) On the difficulty of training recurrent neural networks. In: *International conference on machine learning*, pp 1310–1318
- Porr B, Miller P (2020) Forward propagation closed loop learning. *Adaptive Behavior* 28(3):181–194
- Porr B, Wörgötter F (2003) Isotropic-sequence-order learning in a closed-loop behavioural system. *Philosophical Transactions of the Royal Society of London A: Mathematical, Physical and Engineering Sciences* 361(1811):2225–2244
- Porr B, Wörgötter F (2006) Strongly improved stability and faster convergence of temporal sequence learning by using input correlations only. *Neural computation* 18(6):1380–1412
- Porr B, Wörgötter P (2002) Isotropic sequence order learning using a novel linear algorithm in a closed loop behavioural system. *Biosystems* 67(1-3):195–202
- Porr B, Wörgötter F (2007) Learning with “Relevance”: Using a Third Factor to Stabilize Hebbian Learning. *Neural Computation* 19(10):2694–2719, DOI 10.1162/neco.2007.19.10.2694, URL <https://doi.org/10.1162/neco.2007.19.10.2694>, <https://direct.mit.edu/neco/article-pdf/19/10/2694/816982/neco.2007.19.10.2694>
- Pozzi I, Bohte S, Roelfsema P (2020) Attention-gated brain propagation: How the brain can implement reward-based error backpropagation. *Advances in Neural Information Processing Systems* 33
- Prescott TJ, González FMM, Gurney K, Humphries MD, Redgrave P (2006) A robot model of the basal ganglia: behavior and intrinsic processing. *Neural networks* 19(1):31–61
- Redgrave P, Prescott TJ, Gurney K (1999) Is the short-latency dopamine response too short to signal reward error? *Trends in Neurosciences* 22(4):146–151, DOI [https://doi.org/10.1016/S0166-2236\(98\)01373-3](https://doi.org/10.1016/S0166-2236(98)01373-3), URL <https://www.sciencedirect.com/science/article/pii/S0166223698013733>
- Rehmer A, Kroll A (2020) On the vanishing and exploding gradient problem in gated recurrent units. *IFAC-PapersOnLine* 53(2):1243–1248

- Roberts AC (2011) The importance of serotonin for orbitofrontal function. *Biol Psychiatry* 69(12):1185–91, DOI 10.1016/j.biopsych.2010.12.037
- Rolls ET (2016) Reward systems in the brain and nutrition. *Annual review of nutrition* 36:435–470
- Rolls ET, Grabenhorst F (2008) The orbitofrontal cortex and beyond: From affect to decision-making. *Progress in Neurobiology* 86(3):216–244, DOI <https://doi.org/10.1016/j.pneurobio.2008.09.001>, URL <https://www.sciencedirect.com/science/article/pii/S0301008208000981>
- Schultz W (2004) Neural coding of basic reward terms of animal learning theory, game theory, microeconomics and behavioural ecology. *Curr Opin Neurobiol* 14(2):139–147
- Schultz W (2016) Dopamine reward prediction-error signalling: a two-component response. *Nat Rev Neurosci* 17(3):183–95, DOI 10.1038/nrn.2015.26
- Schultz W, Suri RE (2001) Temporal difference model reproduces anticipatory neural activity. *Neural Comp* 13(4):841–862
- Schultz W, Dayan P, Montague PR (1997) A neural substrate of prediction and reward. *Science* 275:1593–1599
- Shouval HZ, Bear MF, Cooper LN (2002) A unified model of NMDA receptor-dependent bidirectional synaptic plasticity. *Proc Natl Acad Sci (USA)* 99(16):10,831–10,836
- Stork DG (1989) Is backpropagation biologically plausible. In: *International Joint Conference on Neural Networks*, IEEE Washington, DC, vol 2, pp 241–246
- Sutton R (1988) Learning to predict by method of temporal differences. *Machine Learning* 3(1):9–44
- Takahashi YK, Batchelor HM, Liu B, Khanna A, Morales M, Schoenbaum G (2017) Dopamine neurons respond to errors in the prediction of sensory features of expected rewards. *Neuron* 95(6):1395–1405.e3, DOI <https://doi.org/10.1016/j.neuron.2017.08.025>, URL <https://www.sciencedirect.com/science/article/pii/S0896627317307407>
- von Uexküll BJJ (1926) *Theoretical biology*. Kegan Paul, Trubner, London
- Wood J, Simon NW, Koerner FS, Kass RE, Moghaddam B (2017) Networks of VTA Neurons Encode Real-Time Information about Uncertain Numbers of Actions Executed to Earn a Reward. *Front Behav Neurosci* 11:140, DOI 10.3389/fnbeh.2017.00140
- Wörgötter F, Porr B (2005) Temporal sequence learning, prediction and control - a review of different models and their relation to biological mechanisms. *Neural Comp* 17:245–319